PHYSICAL REVIEW D

PARTICLES AND FIELDS

THIRD SERIES, VOLUME 35, NUMBER 1 1 JANUARY 1987

Tests of quantum electrodynamics with two-, three-, and four-photon final states from e^+e^- annihilation at $\sqrt{s}=29$ GeV

E. Fernandez,* W. T. Ford, N. Qi, A. L. Read, Jr., and J. G. Smith
Department of Physics, University of Colorado, Boulder, Colorado 80309

T. Camporesi,† I. Peruzzi, and M. Piccolo
Istituto Nazionale di Física Nucleare, Laboratori Nazionali di Frascati, Frascati, Italy

H. T. Blume, R. B. Hurst, K. H. Lau, J. Pyrlik, J. P. Venuti, H. B. Wald, and Roy Weinstein
Department of Physics, University of Houston, Houston, Texas 77004

H. R. Band, M. W. Gettner, G. P. Goderre, J. H. Moromisato, W. D. Shambroom,‡
J. C. Sleeman, and E. von Goeler
Department of Physics, Northeastern University, Boston, Massachusetts 02115

W. W. Ash, G. B. Chadwick, R. E. Leedy, R. L. Messner, L. J. Moss, F. Muller,§
H. N. Nelson, D. M. Ritson, L. J. Rosenberg, D. E. Wiser, and R. W. Zdarko
Department of Physics and Stanford Linear Accelerator Center, Stanford University, Stanford, California 94305

D. E. Groom and P. G. Verdini
Department of Physics, University of Utah, Salt Lake City, Utah 84112

M. C. Delfino, B. K. Heltsley,** J. R. Johnson, T. L. Lavine, T. Maruyama, and R. Prepost
Department of Physics, University of Wisconsin, Madison, Wisconsin 53706

(Received 23 June 1986)

High-precision measurements of electron-positron annihilation into final states of two, three, and four photons are presented. The data were obtained with the MAC detector at the PEP storage ring of the Stanford Linear Accelerator Center, at a center-of-mass energy of 29 GeV. The measured $e^+e^-\to\gamma\gamma$ differential cross section is used to test the validity of quantum electrodynamics (QED) in this energy range; it agrees well with QED, and the limit on cutoff parameters for the electron propagator is $\Lambda>66$ GeV. The measurement of $e^+e^-\to\gamma\gamma\gamma$ is used to test the QED calculations of order α^3 and to search for anomalies that would indicate the existence of new particles; the agreement with QED is excellent and no anomalies are found. Two events from the reaction $e^+e^-\to\gamma\gamma\gamma\gamma$ are found, in agreement with the QED prediction.

I. INTRODUCTION

The study of electron-positron annihilation into photons provides a very clean test of the validity of quantum electrodynamics (QED) at high energies. This paper presents results from the MAC detector operating at the PEP storage ring of the Stanford Linear Accelerator Center, at a center-of-mass energy ($E_{\text{c.m.}}$) of 29 GeV. The measurements include a high-precision determination of the $e^+e^-\to\gamma\gamma$ differential cross section, measurement of the total cross section for e^+e^- annihilation into three energetic photons, and a study of the kinematic characteristics of this process, and the first published report of annihilation into four energetic photons, a process of order α^4, where α is the QED fine-structure constant.

The reaction $e^+e^-\to\gamma\gamma$ is described by one of the simplest interactions in QED, the electron-photon vertex coupled with the electron propagator.[1] This reaction provides a particularly clean way to test the pointlike behavior of the electron for two reasons: (i) Unlike the photon propagator, the electron propagator does not need vacuum-polarization corrections; (ii) there are no weak-interaction corrections in first-order perturbation theory. Also, the study of $e^+e^-\to\gamma\gamma$ can provide a high-precision measurement of the integrated luminosity ($\int \mathcal{L}\,dt$), allowing the accurate determination of absolutely normalized cross sections for other processes.

As the center-of-mass energy increases, the average en-

ergy of photons emitted in initial- and final-state radiative processes increases, since the photon energy spectrum in these processes is quite similar to a bremsstrahlung spectrum. Since most general purpose detectors are unable to detect photons with energies below a few hundred MeV, direct measurements of QED processes of order α^3 and α^4, such as $e^+e^-\to\gamma\gamma\gamma$ and $e^+e^-\to\gamma\gamma\gamma\gamma$, are possible only at the high energies available at the SLAC storage ring PEP and the similar machine PETRA at DESY. The measurements presented here provide yet a new way to test the validity of QED. These tests are not only important in their own right, but also serve to check on the calculational techniques used to obtain radiative corrections for other processes, such as $e^+e^-\to e^+e^-$ and $e^+e^-\to\mu^+\mu^-$.

II. THE MAC DETECTOR

The MAC detector (Fig. 1) has been described in detail elsewhere.[2] A brief description follows, with emphasis on the components essential to the analysis presented here.

Immediately surrounding the storage ring beam pipe is a 1.9-m-long cylindrical drift chamber (CD), consisting of 10 layers of double-sense-wire drift cells in a 0.57-T axial magnetic field. Six of the layers are tilted 3° with respect to the beam axis to allow measurement of the polar angle through stereoscopic techniques. The drift chamber provides tracking and momentum analysis of charged particles, with typical resolutions of $\sigma(1/p)=0.065\sin\theta$ $(\mathrm{GeV}/c)^{-1}$, $\sigma(\phi)=0.2°$, and $\sigma(\theta)=0.7°$, where p is the momentum of the particle, θ is the polar angle measured with respect to the direction of the incoming positron beam, and ϕ is the azimuthal angle.[3]

Surrounding the CD is an ensemble of finely segmented total-absorption calorimeters, scintillation counters, and outer drift chambers, arranged in a hexagonal prism with end caps. For $|z|<1.2$ m and progressing radially outward, the calorimeter consists of the following.

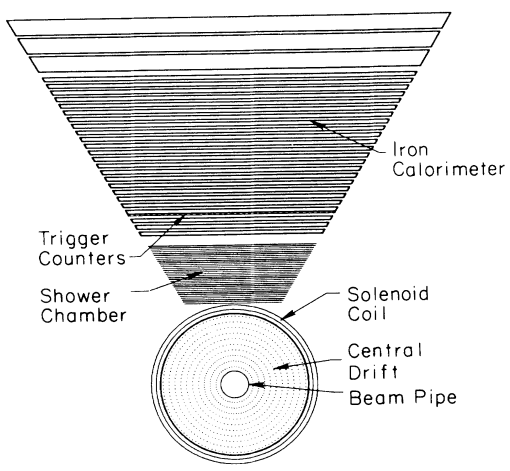

FIG. 1. Section through a sextant of the central part of the MAC detector, illustrating the detector components described in the text.

(1) An electromagnetic shower counter assembled of 32 layers of 2.54-mm-thick lead alloy plates (14 radiation lengths) interleaved with planes of proportional wire chambers[4] (PWC's) whose wire groups are read out at both ends by low-impedance preamplifiers in order to determine the z coordinate by current division. Typical resolutions for electrons in this calorimeter are $\sigma(E)\simeq 0.2\sqrt{E}$, $\sigma(\phi)\simeq 0.6°$, and $\sigma(\theta)\simeq 1.2°$, where E is the particle energy in GeV.

(2) A plane of segmented scintillation counters, used for triggering and time of flight measurement.

(3) A hadron calorimeter assembled from 24 layers of 25.4-mm-thick steel interleaved with PWC's, with typical resolutions for pions of $\sigma(E)\simeq 0.75\sqrt{E}$, $\sigma(\phi)\simeq 1°$, and $\sigma(\theta)\simeq 2°$.

(4) Four planes of cylindrical drift tubes, used to track muons.

For $|z|>1.2$ m the construction is similar except the end-cap electromagnetic calorimeter (EC) consists of 9 layers of 25.4-mm-steel plates interleaved with PWC's with typical resolutions of $\sigma(E)\simeq 0.4\sqrt{E}$, $\sigma(\phi)\simeq 2°$, and $\sigma(\theta)\simeq 1.5°$. The iron calorimeter is magnetized by toroidal coils and forms a muon spectrometer in conjunction with the outer drift tubes.

The two detector elements crucial to the analysis presented here are the electromagnetic shower calorimeter (SC) and the energy-trigger hardware. The actual energy and position resolutions of the SC for high-energy electron and photon showers were measured by analyzing Bhabha-scattering events, which provide a source of electrons of known energy. Averaged over all the data sets collected in two years, the energy resolution for the SC, away from modulate boundaries and after corrections for time-dependent effects such as gas gain, is 6% at $E=14.5$ Gev. A detailed Monte Carlo simulation[5] of the detector predicts $21\%/\sqrt{E}$ resolution (5.5% at 14.5 GeV), in good agreement with the observed value. The energy resolution is slightly worse when the module boundaries are not excluded; this is due to the small uninstrumented regions between sextants and the presence of a small number of dead channels.

The position resolution has been measured with Bhabha electrons, by comparing the angles measured in the CD to those obtained from calorimeter energy clusters, where the cluster angles are obtained from the energy-weighted average of the position information of individual hits. The results for the SC are $\sigma_\phi=0.6°$ and $\sigma_\theta=1.2°$. The ϕ resolution is roughly a factor of 3 better than the hardware segmentation and reflects the fact that the electron shower is shared among several hardware segments. The polar angle resolution is dominated by noise and systematic uncertainties in the calibration of the current division electronics.

The MAC energy trigger uses signals from partial energy sums provided by the preamplifiers in the PWC system. These are summed further to form nine signals: six sextant of SC, one total sum of the central hadron calorimeter, and one sum each for the two end-cap calorimeters. These sums are fed into timing energy discriminators[6] with typical thresholds of 3 GeV. The logical OR of all scintillation-counter signals in the ap-

propriate region of the detector is required to be in coincidence with the central hadron and end-cap calorimeter energy sums, in order to reduce noise effects. The coincidence of any two of nine signals causes readout of the detector electronics.

III. CANDIDATE EVENT SELECTION

Although the detailed criteria for photon identification vary depending on the final state, the general technique used is to require no charged tracks in the CD and an energy-deposition pattern in the calorimeters corresponding to that expected for an electromagnetic shower, with most of the energy deposited in the SC. Candidate events for $e^+e^- \rightarrow$ photons were selected by applying the following cuts to the triggered events accepted by the MAC offline filter program.[7]

(1) No charged tracks must be observed in the CD with an origin consistent with the interaction point (IP).

(2) The ratio of the energy measured in the SC (E_{SC}) to the total energy measured in all the calorimeters (E) must satisfy $E_{SC}/E > 0.70$.

(3) The energy-flow thrust axis[8] must have polar angle $30° < \theta_{thrust} < 150°$.

Requirement (1) selects neutral candidates, accounting for the fact that the presence of a small amount of material between the IP and the CD (beam pipe and inner CD wall, 0.03-rad lengths at normal incidence) will cause a fraction of the photons to convert into an e^+e^- pair or to Compton scatter with an atomic electron. If a photon interacts in the material, the point of origin of the charged tracks will not be consistent with the IP. Requirement (2) selects candidates whose energy deposition is characteristic of electromagnetic showers. Requirement (3) puts a loose cut on the polar angle of the showers in the event; for angles closer than 30° to the beam axis, the CD tracking inefficiency is large enough to create serious background problems from Bhabha-scattering events. This first pass yielded about 10^5 candidates from the raw data accumulated during a 133-pb^{-1} exposure.

The candidates were then processed through a clustering algorithm[9] which gathers the individual calorimeter energy hits into shower clusters. The metric used in the clustering was the space angle between the hits, with the assumption that the shower originated at the IP; it was also required that individual clusters be separated by at least 4° and contain at least two hits. All further analysis is based on the cluster information.

IV. THE REACTION $e^+e^- \rightarrow \gamma\gamma$

In order to extract collinear $\gamma\gamma$ events, the cluster summary information was analyzed requiring (a) at least two and no more than five shower clusters, (b) the energy profile of the two highest-energy clusters (primary clusters) to satisfy $E_{SC}/E > 0.70$ individually, (c) the noncollinearity angle (ξ) between the primary clusters to satisfy $\xi < 10°$, and (d) at least 90% of the clustered energy to be contained in the primary clusters.

Some of the criteria above were developed by studying Bhabha-scattering events, which are copious and have electromagnetic shower characteristics which are virtually identical to the ones for $e^+e^- \rightarrow \gamma\gamma$. The design of the cuts was also guided by the study of simulated $\gamma\gamma$ events, as described below. Figures 2 and 3 illustrate some of the characteristics of the events passing these cuts. Figure 2 shows the distribution of the measured noncollinearity angle (histogram) compared to the expectation of QED theory and the angular resolution of the SC (solid curve). Figure 3 shows a correlation plot of the energies of the primary clusters, showing that the energy is typically concentrated, as expected, in two showers with $E = \frac{1}{2}E_{c.m.}$.

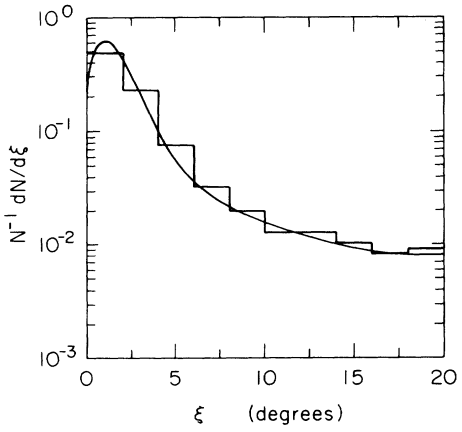

FIG. 2. Distribution of noncollinearity angle for $e^+e^- \rightarrow \gamma\gamma$ events. The histogram represents the data and the solid curve shows the prediction of QED with the angular resolution of the detector folded in.

In order to have a meaningful comparison with theory, effects such as efficiencies and backgrounds must be taken into account; furthermore, at high energies, the theoretical calculations must incorporate higher-order effects. The lowest-order (α^2) cross section for $e^+e^- \rightarrow \gamma\gamma$ can be written as[10]

$$\frac{d\sigma_{\alpha^2}}{d\Omega} = \frac{\alpha^2}{2s}\left[\frac{t}{u}+\frac{u}{t}\right] = \frac{\alpha^2}{s}\frac{1+\cos^2\theta}{1-\cos^2\theta},$$

where s,t,u are the standard Mandelstam variables[11] given by $s = E_{c.m.}^2$, $t = -\frac{1}{2}E_{c.m.}^2(1-\cos\theta)$, and $u = -\frac{1}{2}E_{c.m.}^2(1+\cos\theta)$ in the center-of-mass frame with

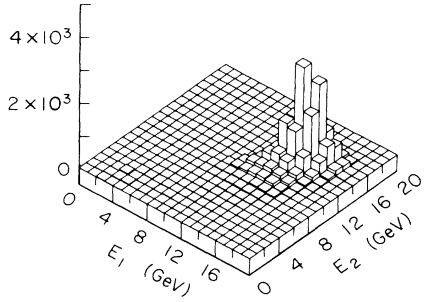

FIG. 3. Correlation between the energies of the primary clusters in $e^+e^- \rightarrow \gamma\gamma$ events, as described in the text.

the approximation $m_e/s \to 0$ (m_e is the mass of the electron). This reaction corresponds to a final state of two collinear ($\xi=0$) photons, each with an energy equal to $\frac{1}{2}E_{\text{c.m.}}$. As shown in Fig. 2, the data has a substantial number of events with $\xi>0$, indicating contributions from higher-order graphs where the incoming e^+ or e^- radiates a photon. The most complete higher-order calculation available in a useful form is the Berends and Kleiss[12] (BK) generator for $e^+e^- \to \gamma\gamma(\gamma)$. The BK program uses a consistent calculation up to terms of order α^3, including virtual corrections and bremsstrahlung. The contributions to the collinear cross section of diagrams with order α^4 and higher are expected to be negligible at our energies.[13]

A sample of $e^+e^- \to \gamma\gamma(\gamma)$ events was generated using the BK generator, corresponding to an integrated luminosity of 269 pb^{-1}. Experimental resolutions, triggering criteria, and analysis efficiencies were simulated on a 34-pb^{-1} subset with the MAC detector simulation program,[5] which produces output with a format identical to actual MAC digital data, allowing the Monte Carlo data to be analyzed with the same programs as the real data. Figure 4 shows the angular dependence of the efficiency $\epsilon(\theta)$ obtained using this procedure; for polar angles away from the θ_{thrust} cut, the efficiency predicted by the simulation has a typical value of 0.94 ± 0.01. Most of the events lost fall into one of the following categories: (1) events with charged tracks in the CD from pair conversions in the beam pipe and inner CD wall; (2) events with photons aimed at uninstrumented regions of the calorimeter which have very low total observed energy; and (3) events with anomalous shower development patterns due to fluctuations or nonuniformities in the calorimeter.

Additional studies of the efficiencies were performed using the data themselves and comparisons of distributions of cut variables between the data and the detector simulation. Good agreement with the predictions of the simulation was observed with the following exceptions: (i) A direct check of the trigger efficiency, from a 35-pb^{-1} subset of the data obtained with a less restrictive single-photon trigger,[14] showed a value of 0.993 ± 0.002, as compared to 1.000 obtained from the simulation; (ii) the efficiency for requiring that at least 90% of the clusters energy be found in the primary clusters was found to be 0.980 ± 0.005, as compared to 1.000 obtained from the simulation. Both of these differences are caused by instrumental problems which are not treated exactly in the detector simulation software, such as the presence of a small number of dead channels in the SC and the effect of multiple track crossings on the SC current division hardware. An overall uncertainty of 1.2% in the absolute value of the efficiencies was estimated from the level of agreement of the data with the Monte Carlo simulation and from studying the sensitivity of the efficiencies to the exact placement of the cuts.

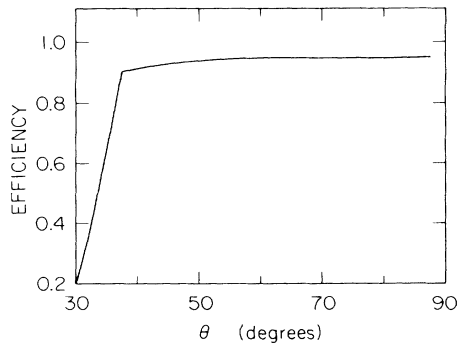

FIG. 4. Detection efficiency for $e^+e^- \to \gamma\gamma$ events as a function of polar angle.

It is convenient to correct the data such that it can be compared directly to the prediction of lowest-order QED. The total observed cross section can be written as

$$\frac{d\sigma_{\alpha^3}}{d\Omega}=\frac{d\sigma_{\alpha^2}}{d\Omega}[1+\delta(\theta)] ,$$

where $1+\delta(\theta)$ is the radiative correction function which is calculated using the Monte Carlo data. Since the efficiencies of all the cuts have been determined separately, it is sufficient for the purposes of this calculation to simulate only the angular resolution functions of the detector. The angular resolution functions of the SC for $40^\circ<\theta<140^\circ$ are simple Gaussians with widths $\sigma_\phi=0.6^\circ$ and $\sigma_\theta=1.2^\circ$, so the angular distribution for this angular range can be calculated with a simplified (and less CPU-intensive) Monte Carlo method. This allows the full use of the 269-pb^{-1} of BK events, minimizing statistical errors. The resulting angular distribution is quite insensitive to changes in the widths of the resolution functions. A change of $\pm0.5^\circ$ alters the contents of each bin by $\pm0.5\%$. For angles closer than 40° to the beam axis the angular resolution function is quite complex, due to the fact that the energy is shared by the SC and EC shower calorimeters, which have different angular segmentations and energy resolutions; the result of the full detector simulation was used for this angular range. Table I summarizes the values of the radiative correction function obtained.

Three possible sources of background have been studied: namely, events coming from random noise in the calorimeters; cosmic rays which shower in the detector; and Bhabha-scattering events which are misidentified in the CD.

In order to study possible random noise effects, the ϕ distribution of events with low total energy ($E<14.5$ GeV) was examined. These events were found to be concentrated at the dead spaces between calorimeter modules, where the detected energy is expected to be anomalously low; the events away from the cracks can be explained by the presence of a few dead electronic channels around the SC calorimeter. Of the 1.37% of events with $E<14.5$ GeV, 90% were found to be either within 5° in ϕ of a calorimeter dead space or within 2 azimuthal segments of a dead electronic channel, leaving a possible noise contamination of $\simeq0.1\%$, quite small compared to the statistical errors.

In order to estimate the cosmic-ray contamination, the $e^+e^- \to \gamma\gamma$ candidates were analyzed requiring a loose coincidence between a cluster of hits in the CD, a scintil-

TABLE I. Summary of radiative-correction calculation for $e^+e^-\to\gamma\gamma$ as obtained from Monte Carlo events. These corrections are specific to the analysis cuts used by this experiment.

θ (deg)	Events	$\int \mathcal{L}\,dt$ (pb^{-1})	σ_{α^3} (pb)	σ_{α^2} (pb)	$1+\delta(\theta)$	Error $(1+\delta)$
37.5	906	33.94	26.69	36.24	0.736	0.024
42.5	7501	268.9	27.88	30.93	0.901	0.010
47.5	6489	268.9	24.12	26.73	0.902	0.011
52.5	5632	268.9	20.93	23.38	0.895	0.012
57.5	4915	268.9	18.27	20.67	0.884	0.013
62.5	4420	268.9	16.43	18.50	0.888	0.013
67.5	4044	268.9	15.03	16.79	0.895	0.014
72.5	3643	268.9	13.54	15.47	0.875	0.014
77.5	3419	268.9	12.71	14.50	0.877	0.015
82.5	3293	268.9	12.24	13.88	0.882	0.015
87.5	3209	268.9	11.93	13.57	0.879	0.016

lator, and a cluster of hits in the outer-drift-chamber system. In a 59-pb^{-1} subsample, 354 events were accepted by the cosmic-ray criteria. These events were visually examined, revealing 12 showering cosmic rays and 342 events with accidental coincidences between a real $e^+e^-\to\gamma\gamma$ event and cosmic-ray tracks or random noise hits in the outer drift chambers. Extrapolating to the full sample yields a background of 0.1%, again very small.

A potentially serious source of background results from the reaction $e^+e^-\to e^+e^-$ (Bhabha scattering). The signature of this process in the calorimeters is virtually identical to that for the $e^+e^-\to\gamma\gamma$ events. To study this background, a subsample of the candidates (68 pb^{-1}) was analyzed requiring the presence of at least one charged track in the CD. The resulting 54 events were visually examined and classified as 46 $e\gamma$, 6 e^+e^-, 1 $\tau\gamma$, and 1 $\gamma\gamma$ with a noise CD track, implying a background of 0.4%. In addition, the detector simulation program was used to estimate the probability of a Bhabha event giving zero tracks (in the region $30°<\theta<150°$) to be less than 10^{-5}, so this background is negligible. The total background was estimated as (0.6 ± 0.2)%.

The experimentally observed differential cross section can be calculated from all the quantities described above. The radiative correction function is included so that the results can be compared to the predictions of first order QED. The corrected cross section is given by

$$\frac{d\sigma}{d\Omega}=\frac{1}{2\pi\Delta\cos\theta}\frac{f_b N(\theta)}{\epsilon(\theta)\epsilon_t[1+\delta(\theta)]\int\mathcal{L}\,dt},$$

where $N(\theta)$ is the number of counts in a θ bin, $f_b=0.994$ is the fraction of the data that is not background, $\int\mathcal{L}\,dt=132.5$ pb^{-1} is the integrated luminosity measured by the MAC small angle luminosity monitor,[2] $\epsilon(\theta)$ is the angular-dependent efficiency in Fig. 4, $\epsilon_t=0.973$ is the overall analysis and trigger efficiency, $1+\delta(\theta)$ is the radiative correction function given in Table I, and $\Delta\cos\theta$ is a solid angle factor for each θ bin.

The results of this calculation are summarized in Table II and displayed in Fig. 5. The statistical error quoted in the table is obtained from the number of counts in each bin using the Poisson distribution. The systematic errors are the contributions from the errors in $\epsilon(\theta)$ and $1+\delta(\theta)$ added in quadrature. The total point-to-point errors shown in Fig. 5 are obtained by combining the previous two errors in quadrature. In addition, there is an overall normalization uncertainty of ±1.2% arising from the errors in f_b and ϵ_t. The top part of the figure shows the corrected angular cross section $d\sigma/d\Omega$ (points with error

TABLE II. Summary of the observed $e^+e^-\to\gamma\gamma$ cross section and errors.

θ (deg)	$d\sigma_{\alpha^2}/d\Omega$ (pb/sr)	Data events	$d\sigma_{\text{expt}}/d\Omega$ (pb/sr)	Statistical error	Systematic error	Total error	% error
37.5	108.41	2887	100.51	1.87	3.49	3.95	3.9
42.5	83.38	3116	78.12	1.41	1.21	1.85	2.4
47.5	66.06	2891	65.21	1.21	1.01	1.57	2.4
52.5	53.69	2527	53.61	1.06	0.96	1.43	2.7
57.5	44.67	2194	43.18	0.93	0.75	1.19	2.8
62.5	38.02	1960	36.94	0.84	0.69	1.09	3.0
67.5	33.12	1779	31.97	0.77	0.65	1.01	3.2
72.5	29.56	1614	28.49	0.70	0.59	0.92	3.2
77.5	27.08	1463	25.64	0.67	0.59	0.90	3.5
82.5	25.51	1431	24.96	0.66	0.60	0.88	3.5
87.5	24.75	1359	22.96	0.62	0.54	0.82	3.6

bars), compared to the prediction of first-order QED (solid line); the normalization has been adjusted as described below. A better way to display the result is shown in Fig. 5(b), where we have formed the ratio of the observed cross section to the QED prediction. The agreement with theory is clearly quite good. The overall normalization was adjusted to fit QED and resulted in a value of

$$\frac{\sigma_{\text{expt}}}{\sigma_{\text{QED}}} = 0.96 \pm 0.009 \pm 0.012 \pm 0.034$$

(with $\chi^2/\text{DF} = 7.8/10$), where the first error results from the point-to-point systematic and statistical errors, the second from the overall normalization uncertainties affecting all data points and the third error is the systematic error in the luminosity measured by the MAC small-angle monitor. The value is clearly consistent with 1.0, the QED prediction.

In order to derive quantitative limits on the validity of QED, it is customary to fit the data to the modified cross section given by[15]

$$\frac{d\sigma}{d\Omega} = \frac{d\sigma_{\text{QED}}}{d\Omega}\left[1 \pm \frac{s^2 \sin^2\theta}{2\Lambda_{\pm}^4 \eta}\right],$$

where $d\sigma_{\text{QED}}/d\Omega$ is the QED differential cross section, $s = E_{\text{c.m.}}{}^2$, $\Lambda_{\pm}$ is a parameter, and η is a function as described below. The subscript on Λ refers to the choice of sign in the equation above. The interpretation of this modification depends on the sign taken and η as follows:

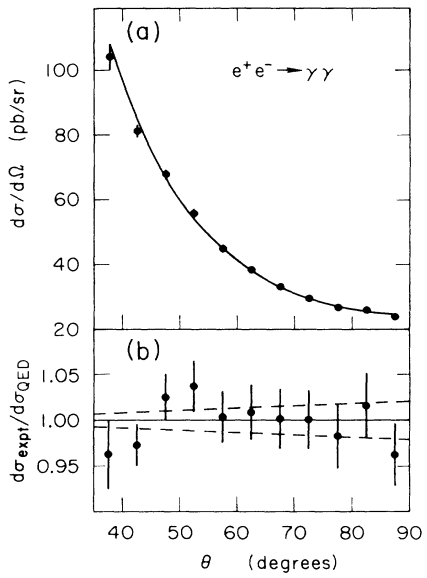

FIG. 5. (a) The measured $e^+e^- \to \gamma\gamma$ differential cross section (points with error bars) compared with the prediction from QED (solid curve). (b) The ratio of the measured distribution to that of QED (points with error bars) compared to the ratios for modified QED with $\eta = 1$ and $\Lambda = 65$ GeV (dashed curves), as described in the text.

$\eta = 1$, sign $= +$: Exchange of a heavy electron with mass M and charge Q ,

where $\Lambda^2 = M^2\left[\frac{e}{Q}\right]$ and e is the electron charge .

$\eta = 1$, sign $= -$: No interpretation .

$\eta = 1 + \cos^2\theta$, sign $= \pm$: The electron propagator itself is modified, indicating a nonpointlike coupling between the electron and the photon; this would arise if the electron had a substructure .

Fits for Λ were performed using both η functions. The modification affects the overall normalization as well as the shape of the angular distribution; to account for this we use a χ^2 function that treats separately the point-to-point errors and the normalization errors.[16] The results of the fit are summarized in Table III and the modified cross sections are illustrated by the dashed lines in Fig. 5(b). No evidence for a breakdown of QED is seen up to $\simeq 65$ GeV, which means that the electron-photon coupling is pointlike down to distances of $\simeq 10^{-18}$ m and that heavy electrons are not likely to exist with a mass less than 65 GeV. Similar limits for the cutoff parameter have been obtained by other experiments, as shown in Table IV. The limits obtained by this experiment are very stringent because of the high accuracy of the measurements and the large solid-angle coverage of the detector.

V. THE REACTIONS $e^+e^- \to \gamma\gamma\gamma$ AND $e^+e^- \to \gamma\gamma\gamma\gamma$

In order to search for a signal from e^+e^- annihilation into more than two photons, events having three or more clusters were examined in more detail. A 92-pb^{-1} subsample of data was used, for which the off-line filter had a high efficiency for these classes of events. Visual examination of a random set of these events showed two large sources of backgrounds which were not associated with the beam: showering cosmic rays and electronic noise in the SC.

In general, both of these backgrounds are characterized by uncorrelated values of total energy (E) and energy imbalance (I_E), defined as

TABLE III. Limits on QED modification parameters for $e^+e^-\to\gamma\gamma$.

η	sign	95% confidence limit on Λ (GeV)	Normalization at minimum	χ^2/DF
1	+	>66	0.938	7.06/9
1	−	>67	0.938	7.06/9
$1+\cos^2\theta$	+	>62	0.931	6.99/9
$1+\cos^2\theta$	−	>64	0.931	6.99/9

$$I_E=\left|\frac{\sum_{i=1}^{n}\mathrm{sgn}[\cos(\psi_i)]E_i}{\sum_{i=1}^{n}E_i}\right|,\quad n=\text{number of clusters},$$

where ψ_i is the angle between the ith cluster and the thrust axis of the event and E_i is the energy of the ith cluster. These features are illustrated in Fig. 6, where the correlation between E and I_E is displayed. The narrow band at imbalance near 1.0 is due to electronic noise whereas cosmic rays populate the zone of moderate imbalance and low total energy. Events from $e^+e^-\to\gamma\gamma\gamma(\gamma)$ should ideally have $E=29$ GeV and $I_E=0$; the requirement (1) 14.5 GeV $<E<$ 40.0 GeV and (2) $I_E<0.90$ eliminate the backgrounds listed above. Another source of background was due to $e^+e^-\to\gamma\gamma$ events in which an extra cluster was found, arising from noise, dead channels, or occasional malfunctions of the current division hardware. This background manifests itself as an excess of events with $\Delta\phi\simeq 0$ and $\xi\simeq 0$, where $\Delta\phi$ is the minimum azimuthal separation between clusters in an event and ξ is the noncollinearity of the two primary clusters. In order to suppress this background, the additional requirement (3) $\Delta\phi>2.5°$ or $\xi>10.0°$ was made.

The 808 events that passed the cuts were inspected visually and classified as 506 background events, 300 events from $e^+e^-\to\gamma\gamma\gamma$, and 2 from $e^+e^-\to\gamma\gamma\gamma\gamma$. The background events are mostly $e^+e^-\to\gamma\gamma$ events with additional energy clusters due to noise, coincidence with a cosmic ray, or errors in the software clustering process; the balance of the background events are showering cosmic rays.

TABLE IV. Comparison of QED-cutoff-parameter results with other experiments. (a) indicates $\eta=1$ was used, (b) indicates $\eta=1+\cos^2\theta$.

Experiment	Limit on Λ_+ (GeV)	Limit on Λ_- (GeV)
MAC	66 (a)	67 (a)
HRS[a]	59 (a)	59 (a)
Mark-J[b]	72 (a)	
TASSO[c]	61 (b)	56 (b)
JADE[d]	61 (b)	57 (b)
CELLO[e]	59 (a)	44 (a)

[a]Reference 17.
[b]Reference 18.
[c]Reference 19.
[d]Reference 20.
[e]Reference 21.

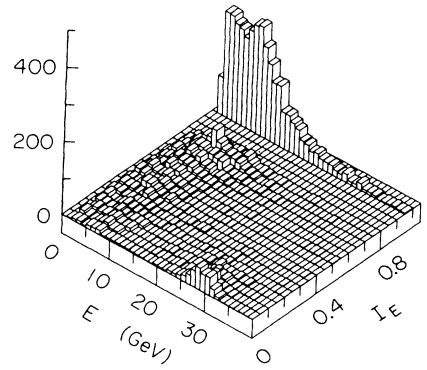

FIG. 6. Energy vs imbalance correlation plot for data events with three or more clusters. Events from $e^+e^-\to\gamma\gamma\gamma$ are expected to cluster at $E\simeq 29$ GeV and $I_E\simeq 0$.

Events with three identified photons were fitted to the $e^+e^-\to\gamma\gamma\gamma$ hypothesis using the kinematics program SQUAW, with the measured energies and angles of the photons as input. About $\frac{2}{3}$ of the events satisfied a four-constraint fit with a confidence level above 5%. The remaining $\frac{1}{3}$ of the events were fitted with three constraints, after removing the measurements with the largest contribution to the χ^2. Of the total of 300 fitted events, 284 events had fits with a confidence level better than 5%. Monte Carlo events from the BK $e^+e^-\to\gamma\gamma(\gamma)$ event generator were processed through the detector simulation and analyzed in exactly the same manner as the real events. All of these Monte Carlo events give fits with confidence level above 5%, due to the fact that some resolutions are slightly underestimated in the simulation.

The measured total cross section for $e^+e^-\to\gamma\gamma\gamma$ into the analysis acceptance is

$$\sigma_{\gamma\gamma\gamma}^{\text{expt}}=(3.2\pm0.2\pm0.1)\text{pb},$$

where the first error is statistical and the second error is due to the uncertainty in the integrated luminosity. The prediction from QED is (3.5±0.1)pb. In order to remove the dependence of the result on the acceptance of the detector, it is best expressed as the ratio of experiment to QED:

$$\frac{\sigma_{\gamma\gamma\gamma}^{\text{expt}}}{\sigma_{\gamma\gamma\gamma}^{\text{QED}}}=0.91\pm0.06\pm0.04,$$

where the systematic error includes the statistical error in the Monte Carlo estimation. The total cross section is in good agreement with the predictions of QED and with other measurements.[22]

The predictions of QED were checked in more detail by examining various kinematic variables. All the data distributions were in excellent agreement with QED. Two

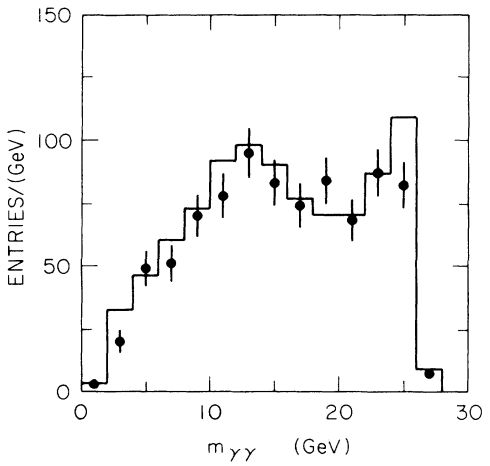

FIG. 7. Invariant-mass distribution for every combination of two photons in $e^+e^-\to\gamma\gamma\gamma$ events (three entries per event). The points with error bars represent the data and the solid histogram is the QED prediction.

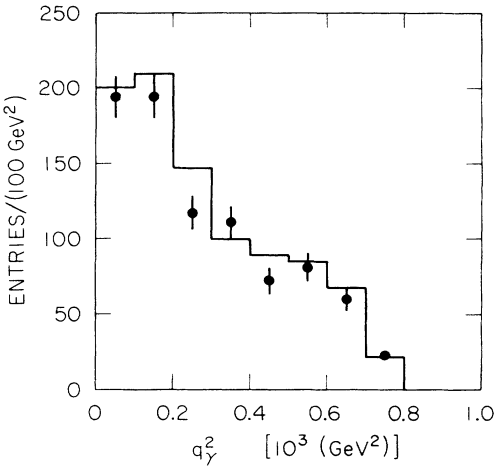

FIG. 8. Momentum-transfer-squared distribution of the photons in $e^+e^-\to\gamma\gamma\gamma$ events (three entries per event). The points with error bars represent the data and the solid histogram is the QED prediction.

examples of kinematic distributions are shown in Figs. 7 and 8, with the data represented by points with error bars and the QED prediction as the solid histogram. Figure 7 shows the invariant-mass distribution of photon pairs; no anomalous deviations with respect to QED are observed. Figure 8 shows the distribution of momentum transfer squared $[q^2=E_{\text{c.m.}}E_\gamma(1-\cos\theta_\gamma)]$, in good agreement with the QED prediction. The kinematic variables plotted for both the data and the Monte Carlo events are calculated using the results of the SQUAW fit.

As mentioned above, two events with four photons in the final state were observed. The parameters of the events are given in Table V; also shown are the angles and energies resulting from a SQUAW fit. Both events give acceptable values of χ^2/DF (0.63/4 and 3.51/4, respectively) in a four-constraint fit using all the measured quantities. The energy of the third photon in event 6728-4951 has a large contribution to the χ^2 and a three-constraint fit using all but that value yields a substantially better fit (χ^2/DF=0.8/3); the energy of the third photon was probably overestimated because of noise in the electromagnetic shower calorimeter. The fitted values quoted in the table correspond to the four-constraint fit in event 6084-8012 and the three-constraint fit in event 6728-4951.

The two observed events correspond to a cross section in the acceptance of 0.02 pb. It is, of course, impossible to study the distributions of kinematic variables with only two events. The QED prediction has been estimated by generating Monte Carlo events with the matrix element of Berends *et al.*[23] and applying to them the full detector simulation and analysis. The predicted number of events into the analysis acceptance is six events. The uncertainty on this predicted number of events is dominated by a systematic error which is difficult to determine, since the theoretical cross section strongly favors events having at least one photon with small polar angle and/or very low energy, where the detector modeling is most uncertain. As the 90%-confidence-level upper limit on two events is

TABLE V. Characteristics of the observed $e^+e^-\to\gamma\gamma\gamma\gamma$ events. The angles are in degrees and the energies in GeV.

			Measured			SQUAW fit		
Run	Event	Photon	ϕ	θ	E	ϕ	θ	E
6084	8012	1	79.2	139.9	12.2	79.2	138.3	11.2
		2	243.4	74.0	9.4	243.4	73.2	10.1
		3	16.8	36.6	6.8	16.8	36.3	6.8
		4	174.1	88.0	0.9	174.1	88.0	0.9
6728	4951	1	29.2	51.9	14.0	29.3	52.4	13.7
		2	222.9	135.9	9.0	222.9	136.4	8.9
		3	223.2	157.4	5.0	223.2	157.4	1.9
		4	187.9	91.2	3.7	187.8	91.3	4.4

5.3, the observed number of events is in reasonable agreement with the prediction of QED and rules out production of four-photon final states from anomalous sources at this sensitivity level.

VI. CONCLUSIONS

Electron-positron annihilation into photons is well described by QED at PEP energies. The $e^+e^-\to\gamma\gamma$ angular distribution and cross section agree well with the theory when radiative corrections up to order α^3 are included. The absence of any deviation from QED sets limits of greater than 67 GeV on the mass scale for QED breakdown. Annihilation into three energetic photons also agrees well with QED in both kinematic distributions and overall rate, providing a check of the theory away from the soft-bremsstrahlung region. Two events with four photons in the final state are observed, consistent with the QED predictions.

ACKNOWLEDGMENTS

We would like to thank R. Kleiss for his help with the calculation of the four-photon final state. We acknowledge the technical assistance and regret the passing of C. T. Pulliam. We also acknowledge the technical assistance of N. Erickson, J. Escalera, M. J. Frankowski and J. Schroeder and the help of J. Kolonko, M. Richards, and J. Richeson. This work was supported in part by the U.S. Department of Energy under Contracts Nos. DE-AC02-81ER40025 (University of Colorado), DE-AC03-76SF00515 (SLAC), and DE-AC02-76ER00881 (University of Wisconsin); by the National Science Foundation under Contracts Nos. NSF-PHY82-15133 (University of Utah), NSF-PHY82-15413, and NSF-PHY82-15414 (Northeastern University), and NSF-PHY83-08135 (University of Utah); and by the Istituto Nazionale di Fisica Nucleare.

---

*Present address: Universidad Autónoma de Barcelona, Barcelona, Spain.

†Present address: CERN, Geneva, Switzerland.

‡Joint appointment: Department of Physics and College of Computer Science, Northeastern University, Boston, MA 02115.

§Permanent address: CERN, Geneva, Switzerland.

**Present address: Laboratory for Nuclear Studies, Cornell University, Ithaca, NY 14853.

[1]See one of the standard textbooks in quantum field theory, such as *Relativistic Quantum Mechanics,* edited by J. D. Bjorken and S. D. Drell (McGraw-Hill, New York, 1964).

[2]E. Fernandez *et al.*, Phys. Rev. D **31**, 1537 (1985); B. K. Heltsley, Ph.D. thesis, July 1983, University of Wisconsin Report No. WISC-EX-83/233; W. T. Ford, in *Proceedings of the Interational Conference on Instrumentation for Colliding Beams,* edited by W. W. Ash (SLAC Report No. SLAC-250, 1982).

[3]The MAC coordinate system is defined as follows: the z axis follows the positron direction in PEP; the x axis points toward the center of the storage ring; and the y axis points upward. The angle ϕ is the azimuthal angle in the x-y plane and θ is the polar angle with respect to the z axis. The differential solid angle $d\Omega$ is given by $2\pi d(\cos\theta)$.

[4]G. Charpak and F. Sauli, Nucl. Instrum. Methods **162**, 405 (1979); F. Sauli, CERN Report No. 77-09, 1977 (unpublished).

[5]The MAC detector simulation program is a detailed geometrical description of the detector, combined with two radiation transport packages: EGS (electron-gamma-shower code) for electron and photon shower simulation, R. L. Ford and W. R. Nelson, SLAC Report No. SLAC 0210, 1978 (unpublished); and HETC (high-energy-transport-code) for hadron showers and muon energy deposition, T. A. Gabriel and B. L. Bishop, Nucl. Instrum. Methods **155**, 81 (1978).

[6]B. Gottschalk, Nucl. Instrum. Methods **190**, 67 (1981).

[7]H. S. Kaye, Ph.D. thesis, Stanford University, 1983, SLAC Report No. SLAC-264.

[8]The thrust is a quantity commonly used to determine the angular orientation of events. The energy-flow thrust axis lies along the unit vector $\hat{\mathbf{T}}$, which is defined as the axis maximizing the thrust T:

$$T\equiv\max_{\hat{\mathbf{T}}}\left[\frac{\sum_i|\mathbf{E}_i\cdot\hat{\mathbf{T}}|}{\sum_i|\mathbf{E}_i|}\right],$$

where the $\mathbf{E}_i$ are the measured energy flow vectors: $\mathbf{E}_i=(E_i,\theta_i,\phi_i)$.

[9]The software package OCLINK from IMSL (International Mathematical and Statistical Libraries, Inc., Houston, Texas) was used.

[10]An excellent introduction to the standard model is given in F. Halzen and A. Martin, *Quarks and Leptons: An Introductory Course in Modern Particle Physics* (Wiley, New York, 1984); also see E. Leader and E. Pedrazzi, *An Introduction to Gauge Theories and the 'New Physics'* (Cambridge University Press, Cambridge, England, 1982).

[11]In a two-body reaction $ab\to cd$ where a,b,c,d are particles described by four-vectors a,b,c,d, the Mandelstam variables are defined as $s=(a+b)^2$, $t=(a-c)^2$, and $u=(a-d)^2$.

[12]F. A. Berends and R. Kleiss, Nucl. Phys. **B186**, 22 (1981).

[13]Y. S. Tsai, Report No. SLAC-PUB 3129, 1983 (unpublished).

[14]E. Fernandez *et al.*, Phys. Rev. Lett. **54**, 1118 (1985).

[15]N. M. Kroll, Nuovo Cimento **A45**, 65 (1966); A. Litke, Ph.D. thesis, Harvard University, 1970.

[16]M. C. Delfino, Ph.D. thesis, December 1985, University of Wisconsin Report No. WISC-EX-85/263.

[17]M. Derrick *et al.*, Phys. Lett. **166B**, 468 (1986); Phys. Rev. D **34**, 3286 (1986).

[18]B. Adeva *et al.*, Phys. Lett. **152B**, 439 (1985); Phys. Rev. Lett. **53**, 134 (1984).

[19]M. Althoff *et al.*, Z. Phys. C **26**, 337 (1984).

[20]W. Bartel *et al.*, Z. Phys. C **19**, 197 (1983).

[21]H. J. Behrend *et al.*, Phys. Lett. **123B**, 127 (1983).

[22]The JADE Collaboration at PETRA reported observation of 195 $e^+e^-\to\gamma\gamma\gamma$ events in Ref. 20. They obtain a value $\sigma^{\rm expt}_{\gamma\gamma\gamma}/\sigma^{\rm QED}_{\gamma\gamma\gamma}=1.10\pm0.08$, where the error is statistical only. No systematic error was quoted.

[23]F. A. Berends *et al.*, Nucl. Phys. **B239**, 395 (1984).